INTERNATIONAL JOURNAL FOR NUMERICAL AND ANALYTICAL METHODS IN GEOMECHANICS, VOL. 20, 647–671 (1996)

NUMERICAL MODELLING OF CONSOLIDATION AND EVAPORATION OF SLURRIED MINE TAILINGS

N. H. SENEVIRATNE

Department of Civil Engineering, University of Peradeniya, Sri Lanka

M. FAHEY, T. A. NEWSON AND Y. FUJIYASU

Department of Civil Engineering, The University of Western Australia, Nedlands, WA 6907, Australia

SUMMARY

Large-strain consolidation theory has been used as the basis of a computer program for dealing with the problem of consolidation of slurried tailings. The work was carried out in the context of the gold-mining industry in Western Australia, where net annual evaporation rates are high (from about 3 to more than 4 m/yr). Therefore, a simple, but effective, method of dealing with evaporation has been included in the model. The paper describes the model, and then uses it with some typical problems to illustrate its versatility and to show the complexity of the behaviour which can occur.

KEY WORDS: tailings; consolidation; evaporation; salinity; numerical modelling

INTRODUCTION

Large quantities of slurried wastes (tailings) produced in modern mining operations are disposed of by sub-aerial deposition in above-ground impoundments. They undergo beaching, followed by large volume changes due to sedimentation, and by consolidation under the combined effects of self weight and evaporative drying, which is particularly significant in arid to semi-arid climates. When the tailings contain significant quantities of clayey fines, the rate of consolidation may be very slow, with consolidation continuing well after disposal has ceased.

In arid and semi-arid regions, there may be conflicting requirements involved in the proper management of a tailings storage area. Thus, the maximum degree of consolidation and hence the maximum stored volume of tailings are obtained by disposing the tailings in thin layers and exposing each layer to evaporation, but a higher rate of return of water to the processing plant may be obtained if disposal is carried out in thicker layers. Similarly, wall stability may be improved, and consolidation enhanced, if the base of the storage is unsealed, but leakage through the base may be unacceptable from an environmental viewpoint.

It is therefore generally necessary to carry out an assessment of the influence on the final state of the storage on various operating procedures and disposal parameters such as base drainage condition, material types, rates and sequences of deposition, potential and actual evaporation rates, etc. Physical modelling and field observations can provide some information, but the ease with which parametric studies can be carried out with a numerical model makes it extremely useful in both the planning and operational stages. Such a model should incorporate large-strain consolidation theory, and should also be capable of dealing with the complexity of disposal

CCC 0363-9061/96/090647-25
© 1996 by John Wiley & Sons, Ltd.
Received 28 June 1995
Revised 2 January 1996

sequences and changes is boundary conditions. The model should also be capable of providing information on strength and density profiles at any time, water volumes lost through evaporation and base seepage, and water volume recoverable by decantation.

This paper describes such a model. The implementation of large-strain consolidation theory is first described. Then, the methods used to model surface evaporation and to apply various boundary conditions are outlined. The capabilities of the model and the complexity of behaviour to be expected are illustrated by applying the model to tailings storages typical of the gold-mining industry in Western Australia (WA).

THEORIES OF SELF-WEIGHT CONSOLIDATION

Simple Terzaghi theory of one-dimensional consolidation is unsuitable for analysing the consolidation of mine tailings because of self-weight forces, and the large deformations which result in substantial variations of material properties (permeability and compressibility). Several mathematical models of one-dimensional large-strain consolidation are described in the literature, see e.g. References 1–4. These models are generally based on either Lagrangian or Eulerian co-ordinate systems. The dependent variable used in the various formulations has included excess or total pore pressure, natural strain, or voids ratio.

Methods have also been developed for dealing with the sedimentation and consolidation behaviour of slurries in a single model (see e.g. Reference 5). However, the work described in this paper has been carried out in the context of the mining industry in WA (mainly the gold-mining industry), where sedimentation is rapid due to sub-aerial deposition. Thus, at this stage, sedimentation is not taken into account explicitly in the model.

Only the Gibson theory of finite-strain consolidation, which is based on a Lagrangian co-ordinate system, is considered in this paper. Convective forces are ignored in this derivation and the motion of pore fluid relative to solids is assumed to be governed by Darcy's law. Unique relationships have been assumed between voids ratio and effective stress and also between permeability and voids ratio. The governing equation of Gibson's theory can be derived as follows.

Consider an element of a soil mass undergoing one-dimensional consolidation from time $t = t_0$ to $t_0 + \delta t$ (see Figure 1). Let the reference variable of the element for the current Lagrangian system be e_0, the voids ratio of the soil element at time t_0. The Lagrangian co-ordinate of the element is a, measured positive vertically upwards from a datum. The vertical equilibrium of the soil element requires that

$$\frac{\partial \sigma_v}{\partial a} + \left(\frac{G_s + e}{1 + e_0}\right)\gamma_w = 0 \tag{1}$$

where e is the voids ratio of the soil at time t, γ_w is the unit weight of water, σ_v is the total vertical stress of the soil at time t, and G_s is the specific gravity of the soil particles.

Considering the vertical equilibrium of the pore fluid leads to the equation

$$\frac{\partial u}{\partial a} = \frac{\partial p}{\partial a} + \left(\frac{1 + e}{1 + e_0}\right)\gamma_w \tag{2}$$

where u and p are the excess and total pore pressures in the soil at time t, respectively. The principle of effective stress can be expressed in differential form as

$$\frac{\partial \sigma_v}{\partial a} = \frac{\partial \sigma'_v}{\partial a} + \frac{\partial p}{\partial a}; \qquad \frac{\partial \sigma_v}{\partial t} = \frac{\partial \sigma'_v}{\partial t} + \frac{\partial p}{\partial t} \tag{3}$$

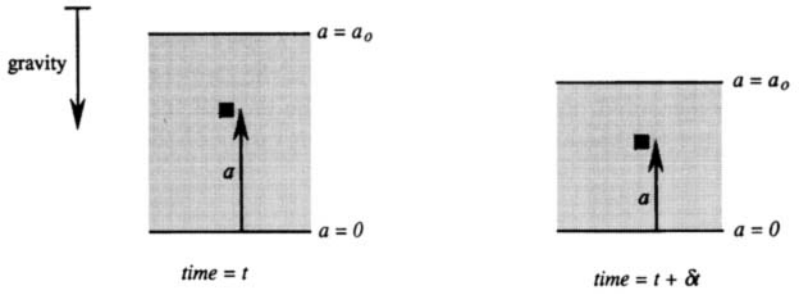

Figure 1. Lagrangian co-ordinate system

Application of Darcy's law gives

$$v = -\left(\frac{k}{\gamma_w}\right)\left(\frac{1+e_0}{1+e}\right)\left(\frac{\partial u}{\partial a}\right) \tag{4}$$

where v is the upward velocity of water flow with respect to soil grains, and k is the permeability of the soil. Continuity of the fluid flow across the soil element requires that

$$\frac{\partial v}{\partial a} = -\left(\frac{1}{1+e_0}\right)\frac{\partial e}{\partial t} \tag{5}$$

Combining equations (2)–(5), the governing equation of self-weight consolidation in Gibson's Theory is obtained as

$$\frac{\partial}{\partial z}\left[\phi\frac{\mathrm{d}\sigma'_v}{\mathrm{d}e}\frac{\partial e}{\partial z}\right] + (G_s - 1)\frac{\mathrm{d}}{\mathrm{d}e}\left(\frac{k}{1+e}\right)\frac{\partial e}{\partial z} = -\frac{\partial e}{\partial t} \tag{6}$$

where $\phi = k/(\gamma_w(1+e))$, and z is the material co-ordinate given by $\mathrm{d}a/\mathrm{d}z = (1+e_0)$.

NUMERICAL MODELLING

The formulation given here is based on an updated Lagrangian co-ordinate system and essentially follows the Gibson model except that total pore pressure is used as the dependent variable instead of voids ratio. This approach is particularly suitable for analysing consolidation problems associated with mine tailings disposal. The surface boundary condition in such problems varies with time as decisions on decantation, etc. are made, depending on the availability of free water on the surface. The specification of such boundary conditions is simpler in terms of the total pore pressure than in terms of the voids ratio.

Equation (6) can be reformulated in terms of the total pore pressure as

$$\frac{\partial}{\partial z}\left[\phi\frac{\partial p}{\partial z}\right] + \frac{\partial k}{\partial z} = \psi\frac{\partial p}{\partial t} - \psi\frac{\partial \sigma_v}{\partial t} \tag{7}$$

where $\psi = -\mathrm{d}e/\mathrm{d}\sigma'_v$. A detailed derivation of equation (7) is given in the Appendix.

The numerical solution of equation (7) for a given boundary value problem is obtained here using a finite element weak formulation for the space variable, coupled with a finite difference

time scheme. Let the soil mass be divided into a number of layers, with nodal points at the boundaries of each layer. Consider the layer i at time t, with the nodal values q_1 and q_2 representing a linear variation of total pore pressure across the element, and z being the element material co-ordinate measured positive upwards from the base of the element. If the material thickness of the layer (i.e. thickness of the layer at zero voids ratio) is h then the total pore pressure p is

$$p = \mathbf{N}_{\mathbf{q}} \tag{8}$$

where $\mathbf{N} = (1 - z/h, z/h)$ and $\mathbf{q}^{\mathrm{T}} = (q_1, q_2)$.

Ignoring the boundary surface integrals which are considered later in the section on boundary conditions, the finite element weak formulation of equation (7) for the layer i is obtained using the Galerkin technique and Green's theorem as

$$\int_0^h \frac{\partial \mathbf{N}^{\mathrm{T}}}{\partial z} \phi \frac{\partial \mathbf{N}}{\partial z} q \, \mathrm{d}z + \int_0^h \frac{\partial \mathbf{N}^{\mathrm{T}}}{\partial z} k \, \mathrm{d}z = -\int_0^h \mathbf{N}^{\mathrm{T}} \psi \frac{\partial p}{\partial t} + \int_0^h \mathbf{N}^{\mathrm{T}} \psi \frac{\partial \sigma_{\mathrm{v}}}{\partial t} \tag{9}$$

(Note that the sign change for the terms on the right-hand sides of equations (7) and (9) is due to the application of Green's theorem). Using a backward time difference scheme of the form

$$q_{t+\delta t} = q_t + \frac{\partial q_{t+\delta t}}{\partial t} \delta t \tag{10}$$

and a single integration point at the centre of the layer, equation (9) for layer i can be expressed as

$$\begin{bmatrix} \bar{\psi}h^2 + 4\bar{\phi}\,\delta t & \bar{\psi}h^2 - 4\bar{\phi}\,\delta t \\ \bar{\psi}h^2 - 4\bar{\phi}\,\delta t & \bar{\psi}h^2 + 4\bar{\phi}\,\delta t \end{bmatrix} q_{t+\delta t} = \begin{bmatrix} 4\bar{k}h\,\delta t + 2\bar{\psi}h^2 \bar{p}_t \\ -4\bar{k}h\,\delta t + 2\bar{\psi}h^2 \bar{p}_t \end{bmatrix} + 2\bar{\psi}h^2 \Delta\bar{\sigma} \begin{bmatrix} 1 \\ 1 \end{bmatrix} \tag{11}$$

In equation (11), $\bar{\phi}$, $\bar{\psi}$ and $\bar{k}$ represent the integration point values at time $t + \delta t$, $\bar{p}_t$ is the total pore pressure at the integration point at time t and $\Delta\bar{\sigma}$ is the increase in the total vertical stress at the integration point during time increment δt. A flow-controlled boundary with an inflow rate of V_n at time $t + \delta t$ is specified by adding a term $4V_n h(\delta t)$ to the right-hand side of equation (11) at the boundary nodes. Equation (11) is not used at the boundaries with prescribed total pore pressure; instead nodal values are directly specified.

The assembly of equations for the layers results in a tri-diagonal set of equations for the nodal variable, the solution of which is straightforward. The solution at time $t + \delta t$ is obtained by successive iterations starting from the values at time t. Equation (11) is updated after each iteration using improved estimations for $\bar{\phi}, \bar{\psi}, \bar{k}$, etc., and the $\Delta\bar{\sigma}$ term is modified after each iteration to accommodate the latest approximation to changes in self-weight stresses during the time increment.

The formulation presented above has been encoded in a computer program called 'MinTaCo' (Mine Tailings Consolidation). The convergence criterion is based on a tolerance for the voids ratio change between successive iterations. If convergence is not reached within 25 iterations, the time increment is halved and the iteration cycle is repeated.

Sudden large changes in the total pore pressures at the boundaries (surface or base) lead to errors in the calculated flow and settlement. This can also occur during filling at the interface between the newly placed material and the existing material. A measure of the accuracy of results

is given by the difference between net outflow of water and total settlement. This difference, which is zero for the exact solution, is printed on the output file by MinTaCo, to provide a check on program performance. In the analyses reported here, this difference is kept at less than 5 per cent of the total settlement. The difference may be reduced by increasing the number of elements used in modelling the problem.

The magnitude of the time increment is found to be critical in ensuring the numerical stability and accuracy of the results. In the MinTaCo program, material properties are assumed to be constant within a time increment. Large time increments lead to substantial changes in strain within an element, and therefore in material properties, causing too much error. In contrast, too small a time increment substantially increases the computation time, though this became necessary for convergence under difficult conditions.

The following procedure was satisfactorily used with the program to minimize the errors in calculation and to improve the numerical stability, without unduly increasing the computation time. An upper limit for time increments is calculated considering the Terzaghi time factor of individual layers as well as the total deposit. The initial value of the first time increment is taken as this upper limit. The initial value for subsequent increments is taken as 150 per cent of the previous time increment (after successful convergence) subject to the above limit. If, after convergence, the increase in strain in any layer exceeds a specified limit, the time increment δt is halved and the iteration cycle is repeated. This constraint is relaxed if the time increment required for convergence becomes too small.

MODELLING OF BOUNDARY CONDITIONS

Base drainage conditions

Various base drainage boundary conditions may be specified in the program. These are:

(1) the base is completely impermeable — i.e. no drainage is permitted through the base;
(2) the base is completely permeable, with a base head being specified — i.e. a pore pressure is specified at the base;
(3) the base is 'leaky' — the tailings are underlaid by a sealing layer of finite thickness and known permeability, with the pore pressure (head) at the base of the sealing layer being specified.

For Cases (2) and (3), the program keeps track of the cumulative flow from the base. This can be useful in calculating seepage to the groundwater, or in estimating the volume of water recoverable from a base drainage system.

Surface boundary conditions

The top boundary surface condition will be described firstly for the case of zero evaporation, and secondly for the case where evaporation is specified.

No evaporation. The top boundary is generally specified to be free draining initially — perhaps with a head of water on the surface, in which case the boundary condition is a particular total pore pressure value. As self-weight consolidation proceeds and water drains to the surface, the depth of water on the surface increases, and this leads to an increase in the boundary total pore pressure. At any stage, decantation of either a set depth of accumulated surface water, or of any

percentage of the accumulated water, can be carried out. Following decantation, the boundary pore pressure is reset to take into account the depth decanted. Conversely, water can be added at the surface at any stage, in which case the depth of accumulated surface water and hence the boundary pore pressure increase. If a layer of fresh tailings is added, the accumulated water from the previous stage is assumed to remain on the top of the fresh layer.

If the base is drained, with a base head lower than the top surface of the tailings, then a stage is eventually reached where the direction of flow through the top surface reverses from being upwards to being downwards. As long as accumulated water remains on the surface, this downward flow continues. However, once the depth of surface water drops at zero, the boundary is set to a zero-flow boundary. From this stage onwards, negative pore pressures can develop in the soil at and below the surface. This suction is permitted to increase up to the point of air entry, as discussed in the next subsection. If, however, a change in conditions results in recommencement of upward flow, the boundary will 'open' again once the suction has reduced to zero.

The result of this is that base drainage can produce some strength right to the surface, even in the absence of evaporation. This is not possible with self-weight consolidation in the case of an undrained base.

With evaporation. Evaporative potential (E_p) in an area is generally described by quoting pan evaporation rates — the rates measured using a Class A evaporation pan. It is generally accepted that evaporation from a bare soil surface is very close to the pan evaporation rate, as long as the soil is fully or nearly fully saturated.

Evaporation in the program is modelled by specifying an evaporative potential — i.e. a depth of water to be removed by evaporation in the current time increment. Evaporation has the same effect as decantation if the sum of the water accumulated on the surface and water flowing to the surface under self-weight consolidation gradients is sufficient to satisfy the evaporative potential. When the evaporative potential cannot fully be satisfied from these sources, the boundary condition is changed. In effect, the hydraulic gradient at the surface is adjusted to give a flow to the surface sufficient to satisfy the evaporative potential. However, the surface suction required to produce this condition is allowed to increase only up to the air-entry suction of the material.

When the air-entry suction is reached, the boundary condition is then specified as a constant-suction boundary, which persists until new material is added. The effect is that the evaporative potential is fully satisfied until this suction limit is reached, and then the actual evaporation rate starts to fall below the potential rate.

In reality, reaching the air-entry suction results in de-saturation of the near-surface material. This produces a rapid drop in permeability, and even though the suction in the water phase continues to increase, the evaporation rate begins to reduce rapidly. Thus, even though the procedure adopted in the program does not model this stage directly, the result is practically the same — i.e. a rapid reduction in the rate of evaporation below the potential rate. This will be illustrated by an example later in the paper.

MATERIAL PROPERTIES

The change in permeability that occurs as the void ratio of a saturated soil reduces due to consolidation was expressed by Carrier *et al.*[6] in the form

$$k = a\frac{e^b}{1+e} \tag{12}$$

where a and b are empirical material constants. Somogyi[7] proposed a similar form that omitted the $1 + e$ (denominator) term, and other forms have also been proposed.

The e–σ'_v relationship of a saturated normally consolidated soil over a large range of voids ratio may be described by a power law of the type

$$e = c(\sigma'_v)^d \tag{13}$$

where c and d are empirical material constants. Carrier *et al.* have shown that the compressibility characteristics of many mineral wastes may be described by similar relationships. Liu and Znidarcic[8] proposed a similar power law, but added a constant to the vertical effective stress term in the brackets. This has the effect of ensuring that the voids ratio is defined even if the effective stress is zero. When a soil is overconsolidated it is convenient to use the classical semi-logarithmic e–σ'_v relationship, i.e.

$$e = e_m - \kappa \ln\left(\frac{p'}{p'_m}\right) \tag{14}$$

where the suffix m refers to a normally consolidated state, and p' is defined by Equation (15) below.

The material parameters for the compressibility and permeability relationships described above may be obtained from consolidation tests. Abu-Hejleh and Znidarcic[9] describe a numerical procedure for determining such parameters using steady-state measurements from a seepage-induced consolidation test. Fahey and Toh[10] describe a procedure based on centrifuge testing. This consists of carrying out a centrifuge test with undrained base conditions. The pore pressure dissipation at the base and the surface settlement are monitored during the test, and the voids ratio profile is determined at the end of the test. The MinTaCo program is used to model the test with values of the four parameters a, b, c and d in equations (12) and (13) being varied until the best match has been achieved with the observed behaviour. This procedure is generally carried out in conjunction with conventional consolidation tests (using a Rowe cell). This gives reliable data at high effective stresses (say 25 kPa and greater), but is difficult to apply to very low effective stresses. However, the behaviour in the centrifuge test is found to be quite sensitive to the forms of the e–σ'_v and k–e relationships at low effective stress, so that the combination of centrifuge and Rowe cell testing is believed to give reliable data over the whole range of effective stress.

Two other material parameters of importance are the air-entry suction value, and the voids ratio at the end of sedimentation. The air-entry suction can be estimated by determining the water content (and hence the voids ratio) at the shrinkage limit. The effective pressure required to achieve the same voids ratio in a conventional (isotropic) compression test is then taken to be equal to the air-entry suction.

The voids ratio immediately after sedimentation may be determined by a simple sedimentation test. In practice, the voids ratio of the slurry as deposited may be very much greater than the sedimentation voids ratio. This is handled in the program by allowing all freshly deposited layers to compress instantaneously to the sedimentation voids ratio, with the excess water generated contributing to the ponded water on the surface or being available for decantation or evaporation.

Knowledge of the shear strength profile of a tailings deposit at any stage during consolidation can be very useful, for example for rehabilitation work which requires surface access for machinery for placement of surface cover layers. Shear strength is not dealt with in the consolidation model. However, since σ'_v is known, and a value for K_0 (the coefficient of earth pressure at rest) can be assumed, then the shear strength can be deduced from the mean effective

stress p', where

$$p' = \frac{(\sigma'_v + 2\sigma'_h)}{3} = \sigma'_v\left(\frac{1 + 2K_0}{3}\right) \tag{15}$$

In the MinTaCo program, the value of K_0 is obtained using the relationships between K_0 and Over-Consolidation Ratio (OCR) described by Mayne and Kulhawy.[11] The undrained shear strength of the soil s_u is determined using the Modified Cam Clay model:[12]

$$s_u = \frac{1}{2} Mp' \exp\left(-\frac{\lambda - \kappa}{\lambda} \log 2\right) \mathrm{OCR}^{(\lambda-\kappa)/\lambda} \tag{16}$$

where M, λ and κ are parameters in the Modified Cam Clay model. The parameter M is the gradient of the critical state line in $q - p'$ space, while λ and κ are the gradients in e–$\ln p'$ space of the virgin compression line and swelling–recompression line, respectively. This form of the relationship is similar to that derived for Cam Clay by Britto and Gunn.[13]

EXAMPLE ANALYSES

The numerical analyses described in this paper were carried out to show the features of the MinTaCo program, and to illustrate the complexity of the behaviour of tailings deposits under the action of self-weight consolidation and evaporation. It is emphasized that the program deals only with individual one-dimensional profiles through a tailings deposit, taking no account of horizontal variability in geometry or material types, and making no allowance for the possibility of horizontal drainage. In practice, sub-aerial deposition of tailings using perimeter spigots results in some sorting of material away from the point(s) of discharge, and formation of a 'beach', and hence in lateral non-homogeneity at any elevation, in addition to vertical non-homogeneity in any profile.

The material parameters used in the analyses were obtained by Toh[14] for clayey silt tailings taken from a gold mine in WA. The values were obtained using centrifuge tests and conventional laboratory consolidation tests, as described above.

For this material, the k–e relationship (equation (12) becomes

$$k\,(\mathrm{m/s}) = 2{\cdot}55 \times 10^{-9}\left(\frac{e^{4{\cdot}1}}{1 + e}\right) \tag{17}$$

and the e–σ'_v relationship (equation (13)) becomes

$$e = 2{\cdot}65(\sigma'_v)^{-0{\cdot}16} \tag{18}$$

where σ'_v is in kPa. These two relationships are illustrated in Figure 2.

In all the cases considered, the tailings storage area is assumed to be 20 m deep. The material is deposited as a slurry at a voids ratio of 4·6. For simplicity, this is also assumed in this case to be the sedimentation voids ratio, so that consolidation starts from this point. The results which will be presented are for the following cases:

(1) The storage area is filled instantaneously, with a slurry at a voids ratio of 4·6. Potential evaporation rates (E_p) of 0·3, 1·5 and 3·0 m/yr are assumed. The base is assumed to be either perfectly drained or perfectly undrained. All surplus surface water not removed by evaporation is decanted, so that no excess water is stored on the surface of the tailings.

(2) The same storage area is filled progressively with the same type of material. The rates of filling are chosen by specifying the rate at which the slurry is added. Filling rates of 4·8, 7·2

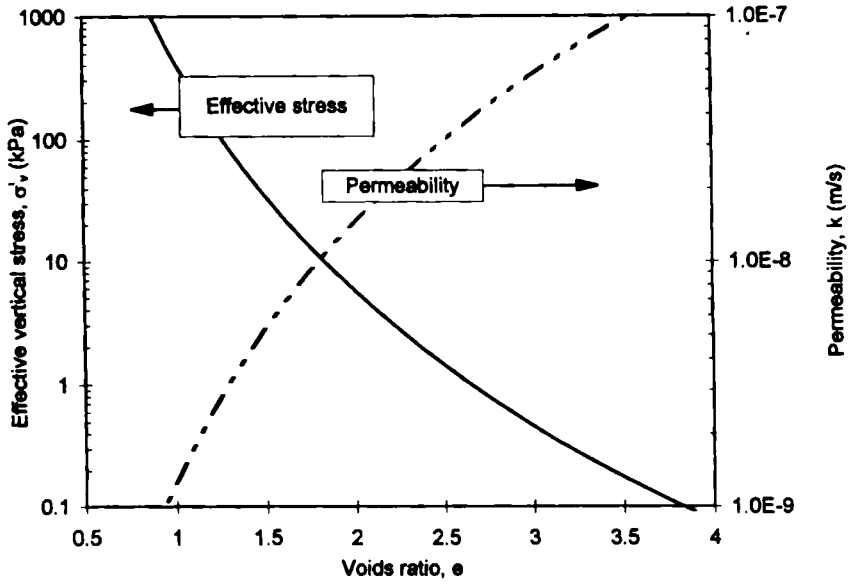

Figure 2. Permeability, voids ratio and effective stress relationships for typical gold tailings

and 9·6 m/yr are used. The base drainage conditions and rates of evaporation considered are identical to those used in the instantaneously filled cases.

The filling sequence in Case 2 actually consisted of adding a layer of the appropriate thickness at the beginning of each month (e.g. 0·4 m/month required to give 4·8 m/yr), and then allowing consolidation, evaporation and decantation to occur during the month until the next filling increment. In the gold-mining industry in WA, the usual practice is to fill area at a constant rate for a certain period (perhaps a month), followed by a consolidation/evaporation period (perhaps 1–3 months). The effects of different deposition and evaporation sequences can be easily examined using the MinTaCo program.

The highest of the three evaporation rates used in these examples represents the conditions which prevail in the arid to semi-arid areas where most of the gold mines in WA are situated. Net average pan evaporation rates in these areas are from 3 m/yr to more than 4 m/yr. Thus, in the method of modelling evaporation described earlier, these are the relevant rates.

However, a complication arises because of salinity. Because of the shortage of fresh water, much of the water used for processing comes from ancient buried river channels ('paleochannels'). Many of these paleochannels connect with the system of salt lakes which are found throughout the region, and hence the salinity of the groundwater can be very high — in many cases as high as 200 g/l (weight of solute per unit volume of solution).

Even moderate salinity can severely reduce the net rate of evaporation. Fahey and Fujiyasu[15] carried our evaporation experiments on slurries of different clay/silt/sand mixes. They stated that whereas the evaporation rate from the non-saline sample was typically about 60 per cent of the potential (i.e. the pan) evaporation rate, this fell to 10 per cent for salinity greater than 5 g/l. Therefore, even in the WA context, it is necessary to evaluate the effects of different evaporation rates, ranging from the very high potential rates of 3–4 m/yr to rates of the order of 10 per cent, or even less, of these rates, resulting from the high salinity. Thus, the lowest of the three evaporation

rates used in the examples (0.3 m/yr) is representative of the true rate that exists when the tailings are highly (or even moderately) saline.

RESULTS AND DISCUSION

Filling rates, evaporation and decantation

Plots of tailings surface height versus time are shown in Figure 3 for different filling rates and a potential evaporation rate (E_p) of 3·0 m/yr. In all cases, the base of the deposit is assumed to be impermeable. The filling rates are 9·6, 7·2 and 4·8 m/yr. These filling rates are the rates at which the slurry is deposited; since consolidation and evaporation occur during filling, the actual rates at which the storage fills are much less, as seen in Figure 3. In all cases, the initial voids ratio is taken as 4·6. The case of the same storage filled instantaneously has also been included for comparison.

Similar plots are shown in Figure 4 for a single filling rate (4·8 m/yr), but three different evaporation rates (0·3, 1·5 and 3·0 m/yr). At an E_p of 0·3 m/yr or 1·5 m/yr, the storage fills at the same rate; it is only after filling is completed that the evaporation rate has an effect on surface height. At an E_p of 3·0 m/yr, the storage fills more slowly and there is practically no ongoing settlement after the completion of filling. Plots for instantaneous filling (the dashed lines), but with the same evaporation rates, are also included in Figure 4.

In each case, the storage is completely filled to 20 m depth. However, the amount of solids deposited is different for each case. This is illustrated in Figure 5, which shows the height of solids stored with time (the height of solids is the height the material would occupy if the voids ratio was zero). At one extreme (with instantaneous filling), the storage contains only 3·57 m of solids, with the rest being water (this reflects the initial voids ratio of 4·6). At the other extreme, with an E_p of 3·0 m/yr and a filling rate of 4·8 m/yr, the total solids height stored is 10·4 m. Thus, the average

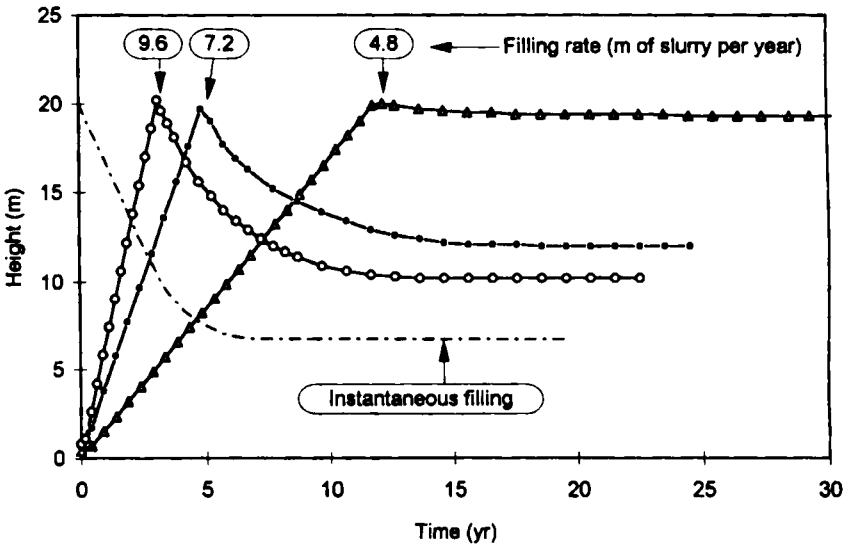

Figure 3. Tailings heights versus time for an E_p of 3.0 m/yr and various filling rates

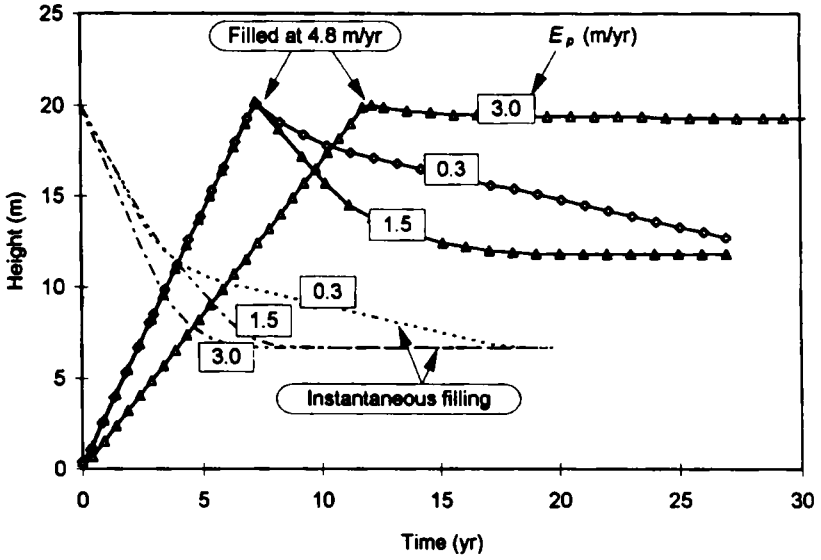

Figure 4. Tailings height versus time for different evaporation rates. Plots shown for instantaneous filling and filling at 4·8 m of slurry per year

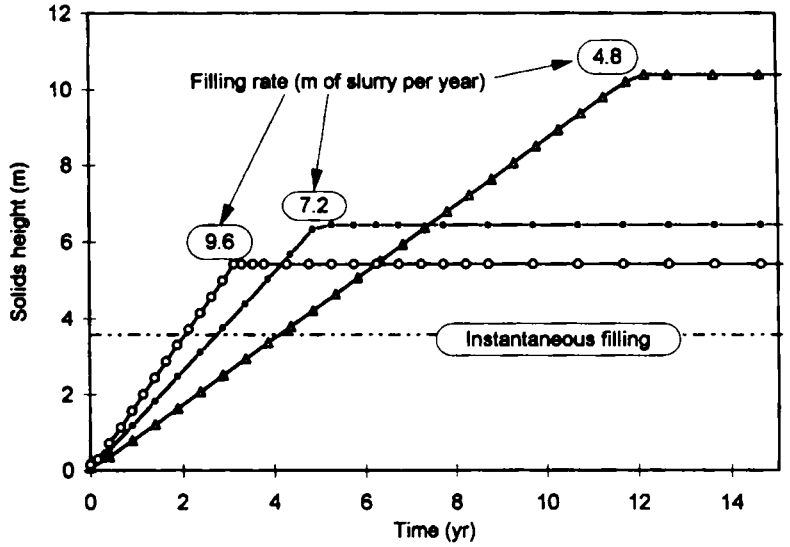

Figure 5. Total solids content (expressed as solids height) versus time for an E_p = 3·0 m/yr and different filling rates

voids ratio in this case is 0·92. Clearly, this is a much more efficient use of the storage, if total storage capacity is the only criterion considered. Of course, filling cannot be instantaneous in reality, but nevertheless it can be fast enough, relative to the consolidation time, to be practically instantaneous.

From Figure 3, it can be seen that at the 4·8 m/yr filling rate, and an E_p of 3·0 m/yr, very little settlement occurs subsequent to filling. However, in all the other cases, significant post-deposition settlement occurs. Thus in all these cases, the efficiency of the storage could be increased by 'topping up' the storage with fresh tailings after significant settlement had occurred.

The effect of this is illustrated in Figures 6 and 7. In Figure 6, the height–time relationships from Figure 3 for two filling rates (4·8 and 9·6 m/yr) are reproduced. Included also is a plot for

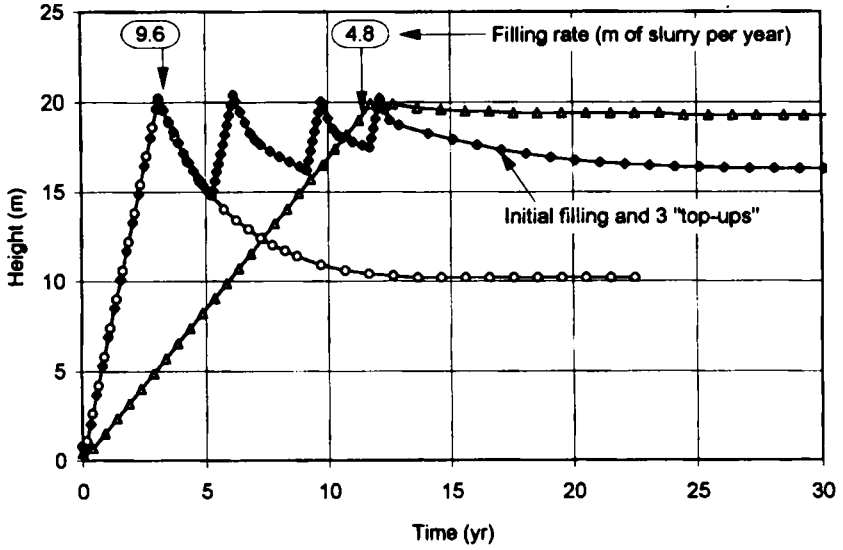

Figure 6. Effect of refilling ('topping up') on surface height, with an E_p of 3·0 m/yr

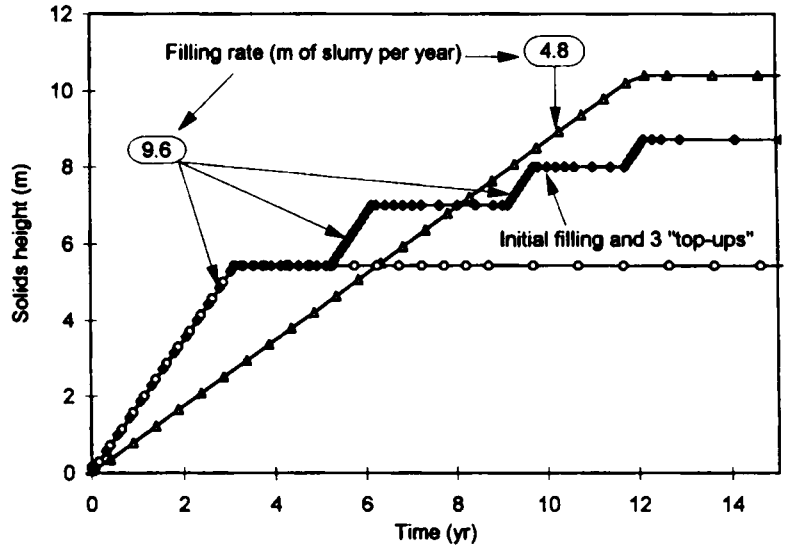

Figure 7. Effect of refilling ('topping up') on solids content, with an E_p of 3·0 m/yr

a filling rate of 9·6 m/yr, where the deposit is 'topped up' three times following the initial filling (in each case topped up at a rate of 9·6 m/yr). The total elapsed time from the start of initial filling to the end of the final topping up is about the same as the total filling time for the 4·8 m/yr filling rate. Consolidation settlement still occurs following the final topping up, but the amount of settlement is very much less than in the case of the same filling rate (9·6 m/yr) where no topping up occurred. Figure 7 shows data from the same cases, plotted as solids height versus time. In this case, the slower rate of filling still achieves the highest total solids content. Nevertheless, the much faster initial filling, followed by repeated top-ups at the same rate, achieves a solids content which is not that much lower (8·7 m compared to 10·4 m for the slow fill rate, or 5·5 m for the fast fill rate with no topping up).

As stated earlier, evaporation is modelled by imposing an evaporation rate at the surface, but only until the air-entry suction is reached at the surface. From that point on, the surface suction is kept constant (until fresh slurry is added). The effect of this can be seen in Figure 8, which shows a plot of cumulative evaporation versus time for various cases, all with an E_p of 3·0 m/yr. The dashed line shows the evaporative potential. In all cases, the actual evaporation rates are almost identical to the potential rate for some time; the differences are due to errors in the numerical modelling. Then, at some stage, the actual rate (i.e. the gradient of the cumulative curve) falls below the potential rate, reducing to practically zero in most cases.

The point at which the actual evaporation starts to fall below the potential rate is when the suction at the surface reaches the air-entry value. As already explained, the program then holds the suction constant at this value, until some circumstance dictates that the suction should be reduced. This is not an accurate model of what happens in practice. In reality, the suction continues to increases, but the permeability begins to reduce dramatically as the soil desaturates. The net effect is that the evaporation rate falls off dramatically. The effect produced in the model (as illustrated in Figure 8) is therefore probably a reasonably good representation of the true behaviour.

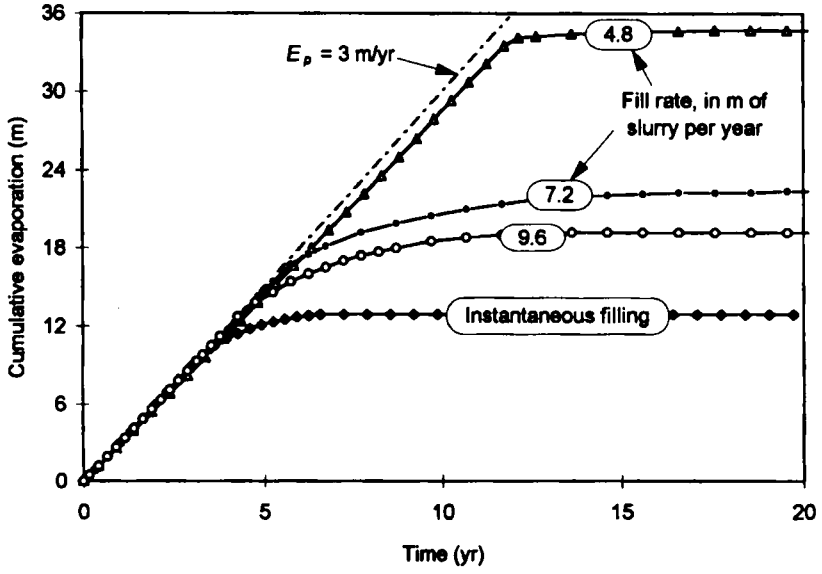

Figure 8. Cumulative evaporation versus time for an E_p = 3·0 m/yr and different filling rates. The dashed line shows the demand rate

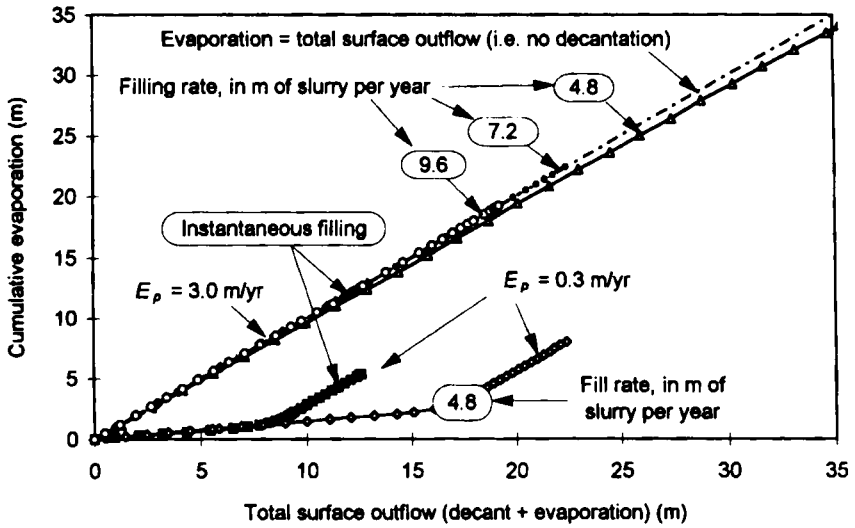

Figure 9. Cumulative evaporation versus total flow from top surface for an E_p = 3·0 m/yr and an E_p = 0·3 m/yr and different filling rates. Vertical offset between plot and dashed line gives quantity decanted

In some of the cases modelled, evaporation has no effect for some time; it simply removes some ponded water that could otherwise be removed by decantation. This is illustrated in Figure 9, which shows the cumulative evaporation plotted against the total top surface outflow (i.e. evaporation plus decantation). The dashed line on this plot is the line of equality, where all surface outflow is taken up by evaporation.

The vertical offset of any plot from this line indicates either the cumulative amount decanted at that stage, or that the actual evaporation rate is less than the demand rate (because the limiting suction is reached). The point at which any plot subsequently becomes parallel to the equality line indicates the point beyond which all water is being taken up by evaporation. Thus, it can be seen that at an E_p of 0·3 m/yr, evaporation only starts to have an effect after about 8 yr for the instantaneously filled case, and after about 16 yr for the case with a filling rate of 4·8 m/yr. Only at these times do the curves become parallel to the equality line, which signifies that there is no surplus water to decant. At an E_p of 3·0 m/yr, there is no decantation at any stage for any of the cases considered.

In all of the cases considered, any water remaining after evaporation is decanted, so no surplus water accumulates on the surface. If this is not done, all accumulated surface water would have to be removed by evaporation before evaporation could start to have an effect on the surface of the tailings, thereby delaying the onset of surface drying.

Pore pressure, voids ratio and shear strength

Pore pressure profiles at different stages are shown in Figure 10 for an E_p of 0·3 m/yr and a rate of filling of 4·8 m/yr. The storage is filled in just over 7 yr, but pore pressures remain positive at all depths until well after this — in fact until about 14 yr. Note that if evaporation is not sufficient to remove surface water, then decantation of this water takes place, so that in this case the pore pressure at the surface is zero until 14 yr. The plot for 18 yr in Figure 10 shows negative

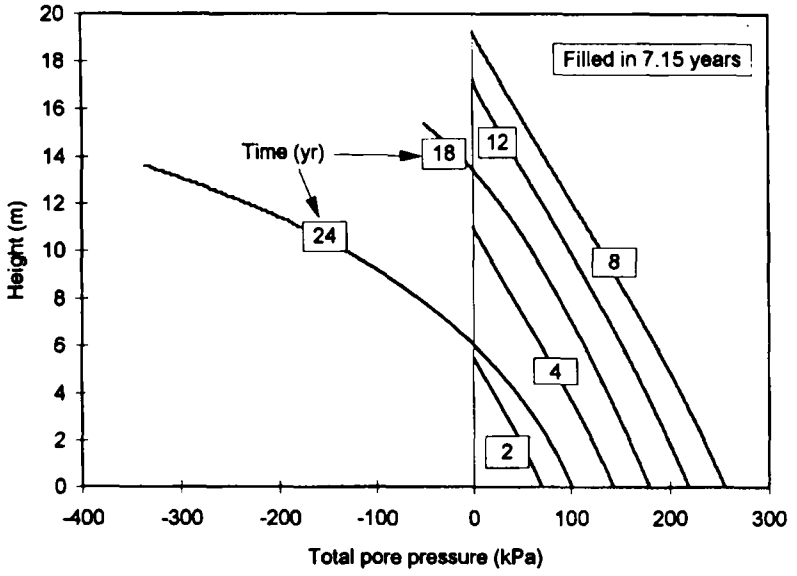

Figure 10. Profiles of total pore pressure at various times after the start of filling, with filling rate of 4·8 m/yr, and an E_p of 0·3 m/yr. Filling to 20 m completed in 7·15 yr

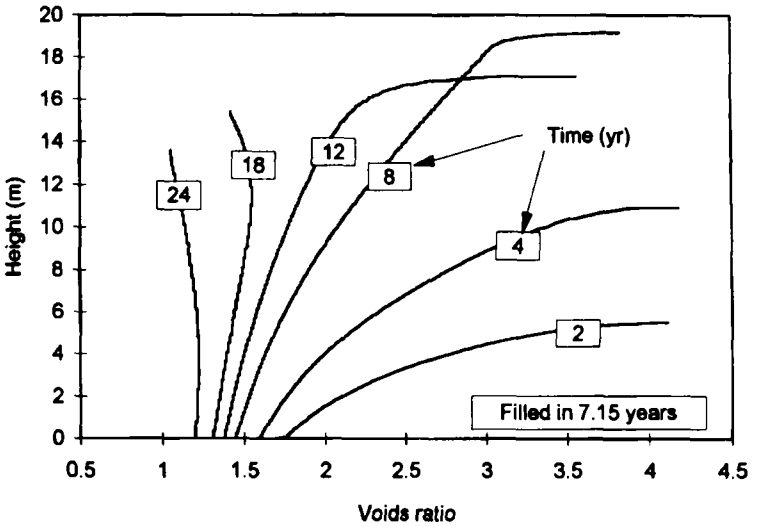

Figure 11. Profiles of voids ratio at various times after the start of filling, for same case as that shown in Figure 10

pore pressures in the upper 2 m only, but by 24 yr, suctions have developed in the upper 8 m or so.

The resulting voids ratio profile is shown in Figure 11. Until the development of surface suction, the voids ratios at the surface remain high. The effect on shear strength can be seen in Figure 12. Self-weight consolidation gives some strength in the lower half of the deposit, but

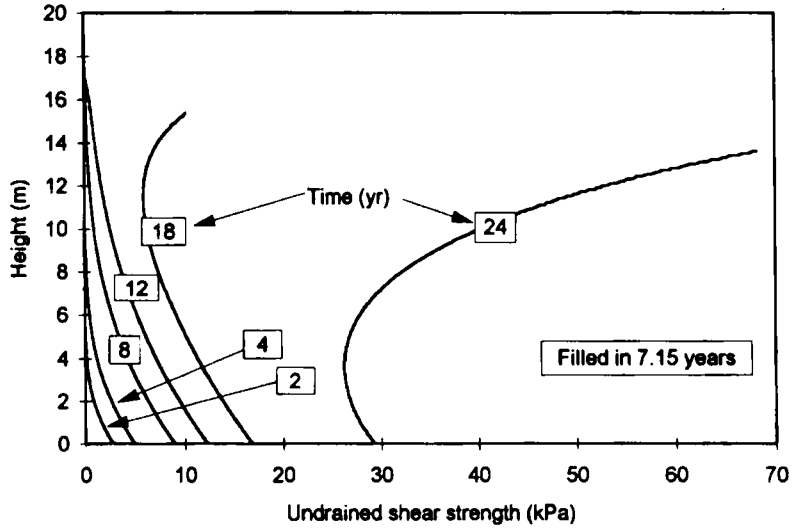

Figure 12. Profiles of undrained shear strength at various times after the start of filling, for the same case as that shown in Figures 10 and 11

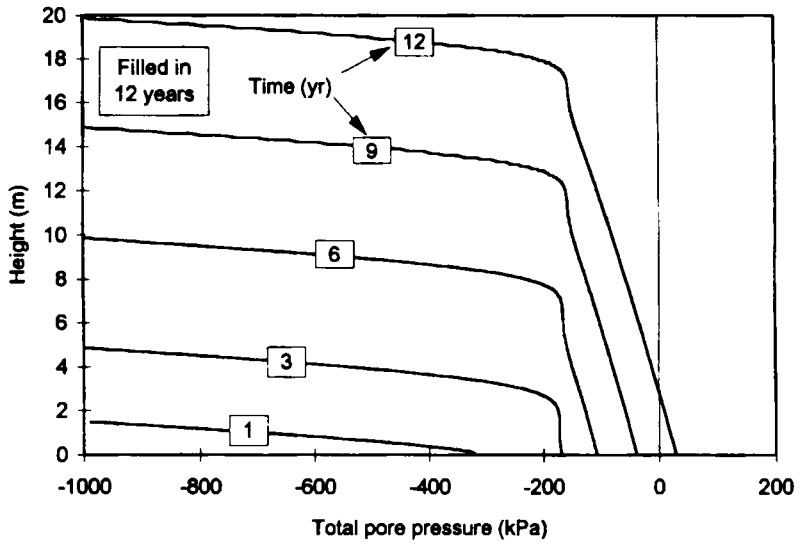

Figure 13. Profiles of total pore pressure at various time after start of filling, filling rate of 4·8 m/yr (as in Figures 10–12) but with an E_p of 3·0 m/yr rather than 0·3 m/yr. Filling to 20 m completed in 12 yr

development of strength at the surface occurs only when evaporation starts to produce surface suctions.

The importance of evaporation is illustrated by comparing these results (in Figures 10–12) with a case where the filling rate is identical (4·8 m/yr), but where E_p is 3·0 m/yr rather than 0·3 m/yr. The pore pressures developed at different stages of filling are shown in Figure 13. In this case, the

air-entry suction (assumed to be 1000 kPa) is reached at the surface at all the time shown except at 1 yr (in all cases, these plots are for the end of a drying phase, just before addition of a fresh layer). Note, however, that the pore pressure at the base of the deposit actually increases with time as more and more slurry is added. Thus, whereas the suction at the top of the deposit at 1 year is almost 1000 kPa, at the same elevation, the suction has reduced to less than 200 kPa at 3 yr. At 12 yr, the pore pressure at this height has become positive.

The resulting voids ratio profiles are shown in Figure 14. Each plot relates to conditions at the end of a drying cycle, just prior to addition of fresh slurry. To understand these plots, it is necessary to consider what happens when a fresh layer of tailings is added. At the end of the previous drying stage, high suctions have built up in the surface layer, with these suctions reducing rapidly with depth. Since the fresh layer is at a high voids ratio, and immediately begins to supply water as it starts to consolidate, the suctions in the underlying material are eliminated almost immediately. Some swelling occurs (increase in voids ratio) in the underlying material, leaving it in a very heavily over-consolidated state. The final voids ratio value for any point therefore depends on how close it was to the top surface during a drying stage, resulting in the peculiar pattern evident in Figure 14.

The resulting shear strength profile for the final stage (at 12 yr) is shown in Figure 15. The strength at any stage depends on the current effective stress state and the past maximum effective stress, in accordance with equation (16). Thus, the high strengths relate to material which was at a drying surface at some stage, and the lower strengths are for material that was below such a surface. (The pattern in this plot is due to the fact that filling occurred by adding four elements, each 0·1 m thick, at monthly intervals). Note that this strength profile assumes that the Modified Cam Clay model adequately represents the softening that occurs when fresh slurry is added. In reality, the softening that occurs may be more severe than indicated here.

For access onto the surface, the most important consideration is the strength at and close to the top of the deposit. The MinTaCa program calculates the average shear strength in the upper 1 m

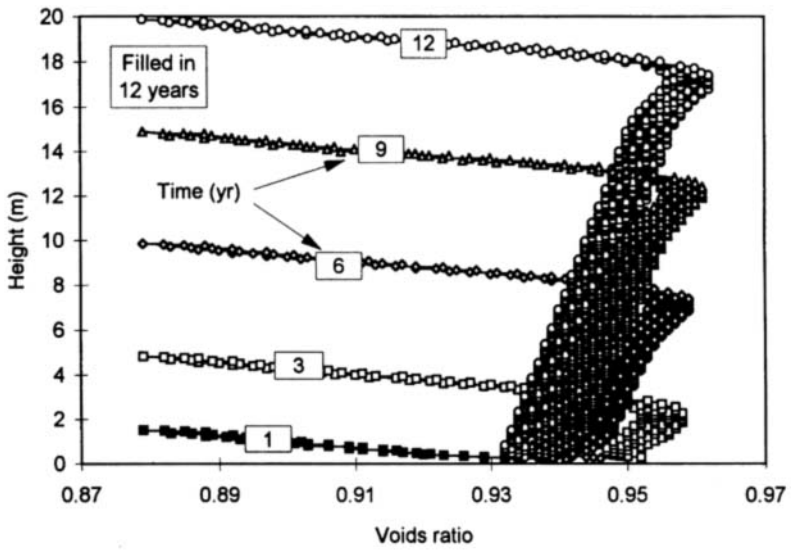

Figure 14. Profiles of voids ratio at various times after the start of filling, for same case as that shown in Figure 13

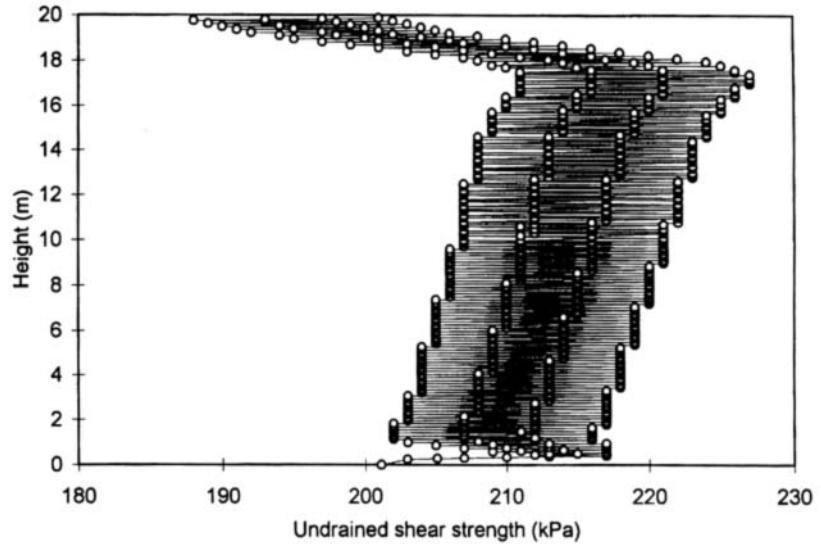

Figure 15. Profile of undrained shear strength at the end of filling, for the same case as that shown in Figures 13 and 14

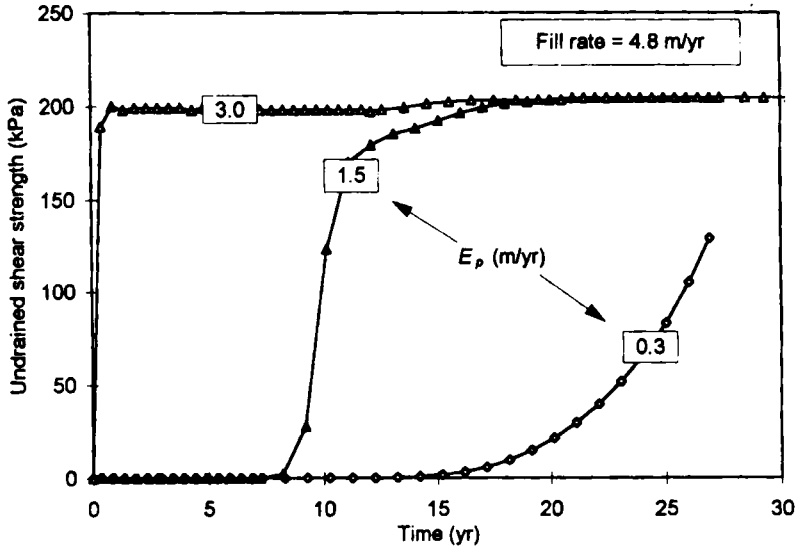

Figure 16. Average shear strength of the upper 1 m of the deposit versus time from the start of filling, for various evaporation rates

of the deposit at each stage, as an indicator of the development of a surface crust. Figure 16 shows the rate at which the strength of this crust develops for E_p values of 0·3, 1·5 and 3·0 m/yr, and a filling rate of 4·8 m/yr. With the highest rate of evaporation, the surface strength is high almost right from the start. However, at the other extreme, almost 14 yr is required for any crust to start

to develop, and it subsequently develops very slowly. (These are the two cases just discussed with reference to Figures 10–12 and 13–15, respectively). At an E_p of 1·5 m/yr, there is no crust until about 10 yr, and then it develops very rapidly (the maximum thickness of 20 m was reached in 7·15 yr for this case). Plots of this type for the other cases modelled show a similar well-defined stage at which the crust develops, so that this types of plot can be very useful in planning rehabilitation work which requires a surface crust of a certain strength.

Since the lowest value of E_p used here (0·3 m/yr) represents the effect of salinity on the potential rate, these results show that salinity can have a dramatic effect on tailings behaviour.

Concept of a 'threshold' filling rate

In the cases discussed in the previous sections, the behaviour seems to fall into two extremes. At one extreme, the evaporation rate is sufficient to achieve high strength and density in the whole profile as filling proceeds, while at the other, evaporation has no effect during filling. The change from one type of behaviour to another occurs over a very narrow range of evaporation rate for a particular filling rate, or over a very narrow range of filling rate for a particular evaporation rate.

Referring to Figure 16, it can be seen that for the three evaporation rates considered in this figure, the highest rate (3·0 m/yr) leads to a very strong surface crust at all stages of filling (and subsequent consolidation), signifying that evaporation has a major influence at the stages of filling. However, for the other two rates, no surface crust develops during filling, with evaporation only starting to have an effect after filling has ceased. Similarly, it was found that at E_p of 3·0 m/yr, a filling rate of 4·8 m/yr is slow enough to allow full consolidation during filling, but the faster rate of 7·2 m/yr previously discussed was too fast to allow this to happen. Further investigation found that a filling rate of 5·3 m/yr was the 'threshold' rate for E_p of 3·0 m/yr. In the same way, for any particular filling rate, the threshold evaporation rate could also be established.

The threshold filling rate (for a given evaporation rate) is important information for the management of a tailings disposal operation, as it indicates the fastest rate that the tailings should be deposited while still allowing evaporation to have its full effect. If filling has to be faster than this rate, then the operator will know that the surface strength will be low at all stages of filling, and that significant post-filling settlement will be likely.

Effect of base drainage

All of the cases considered so far have involved a storage with an undrained base — i.e. a perfectly impermeable base. In practice, the base of a storage may be drained or undrained, or partially drained.

A permeable base has a significant effect on the long-term behaviour of a deposit, particularly in the absence of evaporation, if a low head is maintained in the base drainage system. This results (eventually) in significant effective stresses at the surface, and hence in significant strength.

This is illustrated using a simple case of a 20 m deep storage area, filled instantaneously. The base is fully drained, with a head of 1 m of water in the base drainage layer. Evaporation is assumed to be zero. The behaviour is shown in Figures 17 and 18. In these figures, the dashed lines show the final state for the same case, but with the undrained base.

The initial pore pressure distribution in Figure 17 is equal to the initial total stress. Following deposition, rapid consolidation of the material close to the base occurs. The final distribution is linear, and hydrostatic, leading to a suction of about 70 kPa at the surface. The final distribution

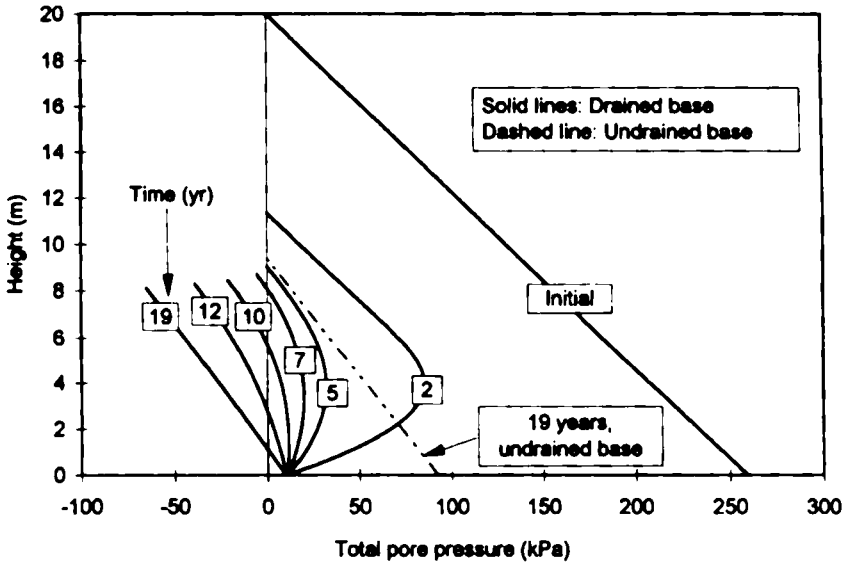

Figure 17. Profiles of total pore pressure for the case of a fully drained base (with a base head of 1 m), with no evaporation. Final profile for undrained base shown for comparison (dashed line)

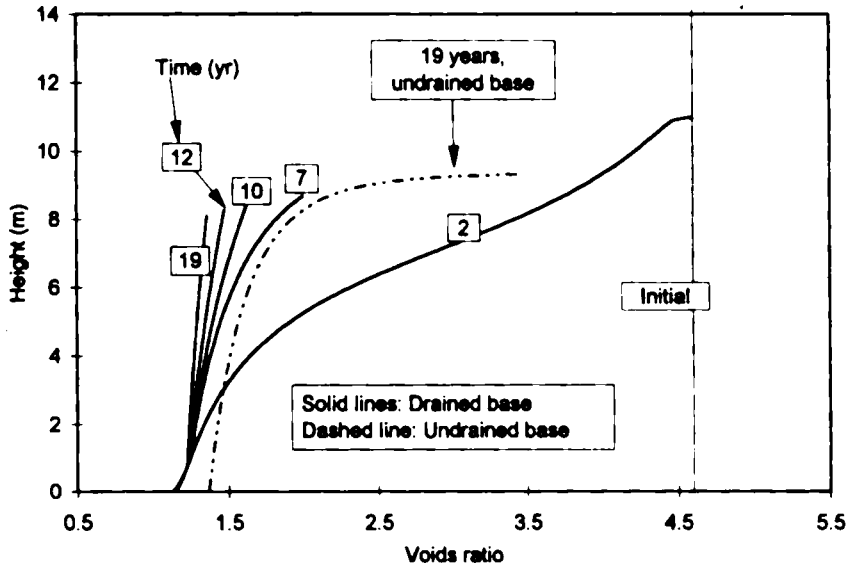

Figure 18. Profiles of voids ratio for the case of a fully drained base (with a base head of 1 m), with no evaporation. Final profile for undrained base shown for comparison (dashed line)

for the undrained case (the dashed line in Figure 17) is also hydrostatic, but with zero pore pressure at the surface.

The resulting profiles of voids ratio are shown in Figure 18. The major benefit of base drainage is seen to be that it eventually produces some consolidation at the surface, and hence a surface

crust, even in the absence of evaporation. However, in practice, it may take a long time for this to occur.

When base drainage is combined with evaporation, the effect of base drainage is less important. Figure 19 shows a comparison between pore pressures with and without base drainage, for the case of filling at 4·8 m/yr and E_p of 3·0 m/yr. With the drained boundary, the base pore pressure (9·81 kPa) is input as a boundary condition, preventing the reduction in base pore pressure evident in the undrained case. The effect of this is that water is actually flowing upwards at the base for much of the analysis, in response to the high upward hydraulic gradient.

In many engineered tailings storages, base drainage systems are incorporated. For such cases, the assumption of a fully drained base is probably appropriate. However, for the storages typical of the gold-mining industry in WA, such cases are rare. Perhaps equally rare are storages with perfectly sealed (undrained) bases. Thus, it would probably be more realistic to model storages with a partially drained base. However, only if the contrast between a perfectly drained and a perfectly undrained case is significant would it be worth trying to model the true base condition explicitly. As already mentioned, the MinTaCo program is capable of modelling 'leaky' bases, but of course obtaining accurate permeability parameters for the base is required for accuracy in this modelling.

Surface cracking

In the modelling work carried out to date, the consolidation process has been treated as a purely one-dimensional one. Thus, all evaporation has been assumed to occur from the top surface, and all shrinkage results in surface settlement only.

In reality, evaporative drying leads to surface cracking. This is apparent in all but the sandiest tailings deposits observed throughout the gold-mining industry in WA. When surface cracks

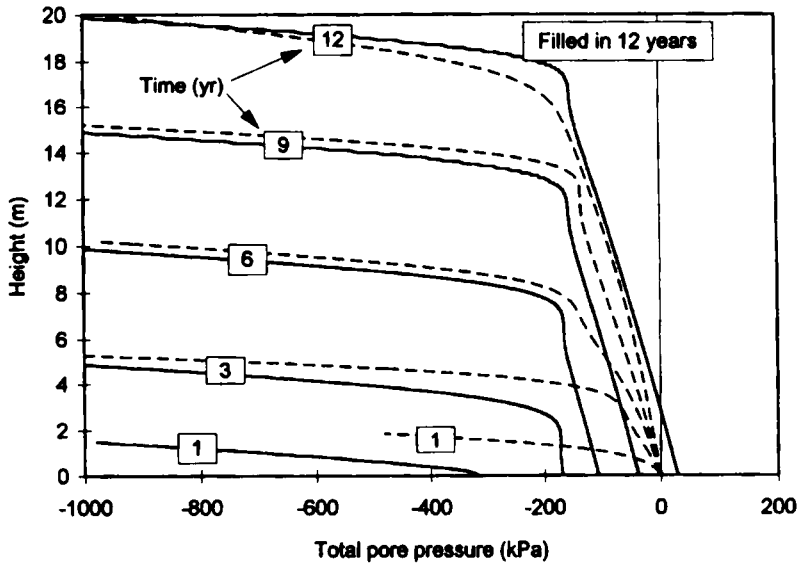

Figure 19. Profiles of total pore pressures at various times for drained base (solid lines) and drained base (dashed lines), both with filling rates of 4·8 m/yr and an E_p of 3·0 m/yr

form, evaporation can potentially occur from the vertical faces of the cracks. The resulting increase in overall evaporation may be very significant, particularly where a surface crust of finer material, formed on the surface in the final stages of sedimentation, tends to inhibit evaporation from the tailings surface.

Surface cracking has not been dealt with specifically in the modelling carried out to date, mainly because sufficient experimental information on evaporation from cracks has not yet been obtained. This is the subject of on-going field and laboratory work.

Nevertheless, it is still possible to make some statements about cracking from the model output. The maximum possible height (H) of a vertical face in a plastic material with a strength of s_u is given by

$$H = \frac{2s_u}{\gamma} \tag{19}$$

where γ is the unit weight of the material. For the case of non-uniform strength and density with depth, this can be reorganized to express the shear strength required to support a crack (a vertical face) of any depth:

$$s_u(z)_{\text{required}} = 0{\cdot}5\,\sigma_z(z) \tag{20}$$

Figure 20 shows a plot of shear strength versus depth for a particular model run (the same case as shown in Figures 10 to 12). As evaporation starts to have an effect, the shear strength increases at the surface, and more slowly below the surface. The relationships represented by equation (20) are also shown in Figure 20 as dashed lines (each line should extend to the origin, but only the relevant section of each line — where it crosses the relevant strength plot — is shown).

Thus, it can be seen that even with only 10 kPa surface strength, the cracks could extend to a depth of almost 1 m. At the final time shown (24 yr), the cracks could be about 4 m deep.

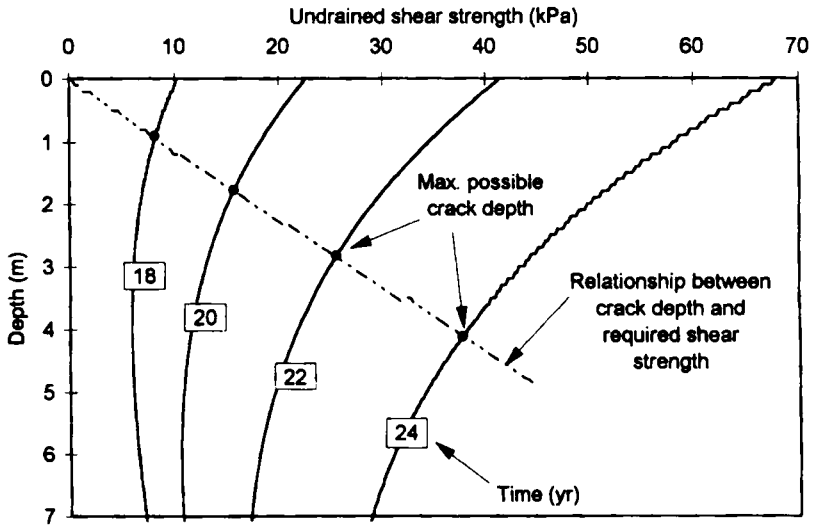

Figure 20. Shear strength versus depth profiles at various stages (filling rate = 4·8 m/yr, E_p = 0·3 m/yr), showing maximum possible crack depth at each stage

Note that this is not meant to be a model for predicting crack depths. Where tailings are deposited in layers, with each layer being allowed to dry before the next is deposited, any cracks developing in a layer will be filled with fresh slurry when the next layer is added. The potential shrinkage of layers that have already undergone a drying–wetting cycle is much less than that of fresh layers, so that the potential for deep cracking is limited in such deposits. Thus, for the case shown in Figure 15, cracking would probably occur only in the top layer at any stage of filling, whereas a simplistic application of equation (20) would suggest that very deep cracking was possible in this deposit. However, if tailings are deposited in very thick layers (or where drying of individual thin layers is not permitted during deposition), deep cracking is possible and does occur, particularly where the clay content is high. Under these circumstances, the approach outlined would be useful in giving the maximum potential crack depth.

CONCLUSION

The use of large-strain consolidation theory to model the consolidation behaviour of slurried mine tailings has become commonplace over the past couple of decades. However, in the WA context, the high natural evaporation rates of the area are a major factor in the management of gold tailings storages, and thus the capability of modelling evaporation must be included in any numerical modelling scheme.

This paper describes a computer code (MinTaCo) which has been developed to model one-dimensional consolidation of tailings in this environment. A method of including evaporation has been described, which, though very simple, allows the effects of evaporation to be evaluated realistically. Being one-dimensional, the model can only deal with horizontal non-homogeneity in the tailings by modelling different vertical profiles representing different areas within the tailings storage area. The examples presented show the versatility of the model and the complexity of the behaviour, even when the complications of horizontal or vertical non-homogeneity are not considered.

ACKNOWLEDGEMENTS

The work described in this paper was supported by grants from the Australian Research Council (ARC) and the Minerals and Energy Research Institute of Western Australia (MERIWA). The first author was supported during a sabbatical leave at The University of Western Australia by a Fellowship from the Geomechanics Group at UWA. The fourth author was supported by an Overseas Postgraduate Research Studentship from the Commonwealth Government of Australia and by a UWA Geomechanics Group studentship.

APPENDIX

The detailed derivation of equation (7) is given below.

Equations (1) and (3) can be expressed in terms of material co-ordinate z as

$$\frac{\partial \sigma_v}{\partial z} + (G_s + e)\gamma_w = 0 \tag{21}$$

$$\frac{\partial \sigma_v}{\partial z} = \frac{\partial \sigma'_v}{\partial z} + \frac{\partial p}{\partial z} \tag{22}$$

Using equation (22)

$$\frac{\partial}{\partial z}\left[\phi\frac{d\sigma'_v}{de}\frac{\partial e}{\partial z}\right]=\frac{\partial}{\partial z}\left[\phi\frac{\partial\sigma'_v}{\partial z}\right]=\frac{\partial}{\partial z}\left[\frac{k}{\gamma_w(1+e)}\frac{\partial\sigma_v}{\partial z}\right]-\frac{\partial}{\partial z}\left[\phi\frac{\partial p}{\partial z}\right] \tag{23}$$

But, using equation (21), the first term on the right-hand side of (23) can be written as

$$\frac{\partial}{\partial z}\left[\frac{k}{\gamma_w(1+e)}\frac{\partial\sigma_v}{\partial z}\right]=\frac{\partial}{\partial z}\left[\frac{-k}{(1+e)}(G_s+e)\right]=\frac{\partial}{\partial z}\left[-k-(G_s-1)\frac{k}{1+e}\right]$$

$$=-(G_s-1)\frac{\partial}{\partial z}\left[\frac{k}{1+e}\right]-\frac{\partial k}{\partial z} \tag{24}$$

Substituting this into equation (23) gives

$$\frac{\partial}{\partial z}\left[\phi\frac{d\sigma'_v}{de}\frac{\partial e}{\partial z}\right]=-(G_s-1)\frac{\partial}{\partial z}\left[\frac{k}{1+e}\right]-\frac{\partial}{\partial z}\left[\phi\frac{\partial p}{\partial z}\right]-\frac{\partial k}{\partial z}$$

which gives

$$\frac{\partial}{\partial z}\left[\phi\frac{d\sigma'_v}{de}\frac{\partial e}{\partial z}\right]+(G_s-1)\frac{d}{de}\left[\frac{k}{1+e}\right]\frac{\partial e}{\partial z}=-\frac{\partial}{\partial z}\left[\phi\frac{\partial p}{\partial z}+k\right] \tag{25}$$

Since the left-hand sides of equations (6) and (25) are equal, then the right-hand sides are also equal:

$$\frac{\partial}{\partial z}\left[\phi\frac{\partial p}{\partial z}+k\right]=\frac{\partial e}{\partial t} \tag{26}$$

Using equation (3),

$$\frac{\partial e}{\partial t}=\frac{de}{d\sigma'_v}\frac{\partial\sigma'_v}{\partial t}=-\psi\frac{\partial\sigma'_v}{\partial t}-\psi\left[\frac{\partial\sigma_v}{\partial t}-\frac{\partial p}{\partial t}\right]=\psi\frac{\partial p}{\partial t}-\psi\frac{\partial\sigma_v}{\partial t} \tag{27}$$

Substituting this into equation (25) gives equation (7).

REFERENCES

1. M. Miksa, 'The consolidation of soft clay, a new consolidation theory and its application', in *Japanese Society of Civil Engineers*, 1965, pp. 21–26 (Reprint from Civil Engineering in Japan, 1965).
2. R. E. Gibson, G. L. England and M. J. L. Hussey, 'The theory of one-dimensional consolidation of saturated clays, I. Finite non-linear consolidation of thin homogeneous layers', *Géotechnique*, **17** (3), 261–273 (1967).
3. R. E. Gibson, R. L. Schiffman and K. W. Cargill, 'The theory of one-dimensional consolidation of saturated clays, II. Finite non-linear consolidation of thick homogeneous layers', *Can. Geotech. J.*, **18** (2), 280–293 (1981).
4. S. D. Koppula and N. R. Morgenstern, 'On the consolidation of sedimenting clays', *Can. Geotech. J.*, **19** (2), 260–268 (1982).
5. V. Pane and R. L. Schiffman, 'A note on sedimentation and consolidation',*Géotechnique*, **35** (1), 69–72 (1985).
6. W. D. Carrier, L. G. Bromwell and F. Somogyi, 'Design capacity of slurried mineral waste ponds', *J. Geotech. Eng. Div.* ASCE, **109** (GT5), 699–716 (1983).
7. F. Somogyi, 'Analysis and prediction of phosphatic clay consolidation: implementation package; *Technical Report*, Phosphatic Clay Research Project, Lakeland, Florida, 1979.
8. J. C. Liu and D. Znidarcic, 'Modelling one-dimensional compression characteristics of soils', *J. Geotech. Eng. Div.* ASCE, **117** (GT1), 162–169 (1991).
9. A. N. Abu-Hejleh and D. Znidarcic, 'Estimation of the consolidation constitutive relations', in H. J. Siriwardane and M. M. Zaman (eds.), *Proc. 8th Int. Conf. on Computer Methods and Advances in Geomechanics*, Vol. 2, Balkema, Rotterdam, 1994, pp. 499–504.

10. M. Fahey and S. H. Toh, 'A methodology for predicting the consolidation behaviour of mine tailings', in T. Szwedzicki et al. (eds.), *Proc. Western Australian Conf. on Mining Geomechanics*, Kalgoorlie, Western Australia, Curtin University of Technology, Perth, Australia, (1992) pp. 445–452.
11. P. W. Mayne and F. H. Kulhawy, 'K_0–OCR relationships in soil', *J. Geotech. Eng. Div.* ASCE, **108** (GT6), 851–872 (1982).
12. K. H. Roscoe and J. B. Burland, 'On the generalised stress-strain behaviour of wet clay', in J. Heyman and F. Leckie, (eds.), *Engineering Plasticity*, Cambridge University Press, Cambridge, 1968.
13. A. M. Britto and M. J. Gunn, *Critical state soil mechanics via finite elements*, Ellis Horwood, Chichester, U.K., 1987.
14. S. H. Toh, 'Numerical and centrifuge modelling of mine tailings consolidation', *Ph.D. Thesis*, The University of Western Australia, 1992.
15. M. Fahey and Y. Fujiyasu, 'The influence of evaporation on the consolidation behaviour of gold tailings', in Technical Program Committee, W. D. Carrier (Chairman) (ed.), *Proc. 1st Int. Congress on Environmental Geotechnics*, Edmonton, Alberta, Canada, 1994, 481–486.